ISBN: 978-3-95450-231-8 ISSN: 2673-5490 doi: 10.18429/JACoW-IPAC2023-WEPL189

SIMULATION STUDIES ON LONGITUDINAL BEAM DYNAMICS MANIPULATED BY CORRUGATED STRUCTURES UNDER DIFFERENT BUNCH LENGTH CONDITIONS AT KARA

S. Maier*, M. Brosi†, H. J. Cha, A. Mochihashi, M. J. Nasse, P. Schreiber‡, M. Schwarz, A.-S. Müller, Karlsruhe Institute of Technology, Karlsruhe, Germany

Abstract

In the KIT storage ring KARA (KArlsruhe Research Accelerator), two parallel plates with periodic rectangular corrugations are planned to be installed in a dedicated part of the vacuum chamber. These plates will be used for impedance manipulation to study and eventually control the beam dynamics and the emitted coherent synchrotron radiation (CSR). In this contribution, we present simulation results showing the influence of different corrugated structures on the longitudinal beam dynamics and how this influence depends on the machine setting in the low momentum compaction regime.

INTRODUCTION

In contrast to incoherent synchrotron radiation, coherent synchrotron radiation (CSR) scales quadratically and not linearly with the number of emitting particles. Consequently, the emitted photon flux can be amplified by several orders of magnitude. For the generation of CSR pulses in the THz frequency range, the length of the emitting structure has to be reduced to the single-digit picosecond time scale since the radiation is only coherent if the wavelength of the emitted photons is longer than the radiating structure.

At KARA, this longitudinal compression of the bunches is realized using a magnetic lattice with reduced momentum compaction factor (low-α_C) [1,2]. The resulting high particle density entails nonlinear phenomena due to the interaction of the particle bunches with their self-emitted CSR. This can result in longitudinal bunch deformations and dynamical fluctuations, due to the microbunching instability. The latter causes longitudinal substructures on the bunches and generates quasi-periodic outbursts of intense THz radiation [1,3,4]. The understanding of this instability is crucial for opening a new additional frequency range with intense radiation for various experiments, which were not possible previously.

A versatile impedance manipulation chamber is currently under development for the KARA storage ring at KIT. Changing the longitudinal impedance of the ring and the longitudinal wakefields of the particles influences the beam dynamics of the passing electrons. The additional impedance and the change of wakefields are created by a pair of horizontal parallel plates with periodic rectangular corrugations perpendicular to the propagation direction of the electrons. Figure 1 shows a schematic cross section of the structure

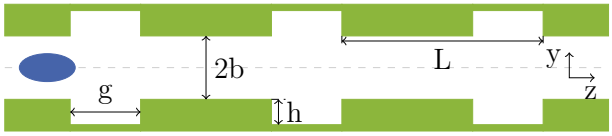

Figure 1: Corrugated plates in cross section with the relevant geometric parameters. The blue ellipse indicates an electron bunch.

with geometric parameters corrugation depth h, periodic length L, corrugation width g, and plate distance $2b$. To our knowledge, such a structure has not yet been installed into a storage ring. At KARA, the bunch profile and the emitted CSR can be affected periodically by the additional impedance due to the repeated passage with the revolution frequency of 2.7 MHz.

The longitudinal impedance $Z^{\parallel}$ of a cylindrical corrugated pipe has been theoretically described in Ng *et al.* [5] with the validity range $L \lesssim h \ll b$, as

$$\frac{Z^{\parallel}}{L} = \frac{Z_{\mathrm{vac}}}{\pi b^2}\left[\pi k_{\mathrm{res}}\delta\left(k^2 - k_{\mathrm{res}}^2\right) + i \cdot \mathrm{P.V.}\left(\frac{k}{k^2 - k_{\mathrm{res}}^2}\right)\right] \quad (1)$$

with the resonance wave number $k_{\mathrm{res}} = \sqrt{\frac{2L}{bgh}}$, the wave number $k = \frac{\omega}{c}$, the vacuum impedance Z_{vac}, the δ-distribution, and the principal value P.V.(x) [6]. In [7], we already confirmed a good agreement between the simulation results and the theoretical prediction of the impedance.

This contribution shows the impact of different impedances on the beam dynamics depending on the machine parameters, namely the momentum compaction factor α_c and the acceleration voltage V_{acc}.

IMPEDANCE SCAN

The longitudinal beam dynamics have been simulated with the in-house developed Vlasov-Fokker-Planck solver Inovesa [8], for which a good agreement with measurements of the microbunching instability at KARA has already been shown [9].

In the following, the machine settings are changed by adjusting α_c and $V_{\mathrm{acc.}}$. In all simulations, the overall impedance is given by the dominant CSR parallel plate impedance [10] at KARA and the additional impedance of the corrugated structure, which is determined by the resonator model [11] with its resonance frequency f_{res}, shunt impedance Z_0, and quality factor Q. As only the impact of the resonance frequency is examined, the latter two parameters remain fixed

* sebastian.maier@kit.edu
† Now at MAX IV Laboratory, Lund, Sweden
‡ Now at Synchrotron SOLEIL, Saint-Aubin, France

ISBN: 978-3-95450-231-8 ISSN: 2673-5490 doi: 10.18429/JACoW-IPAC2023-WEPL189

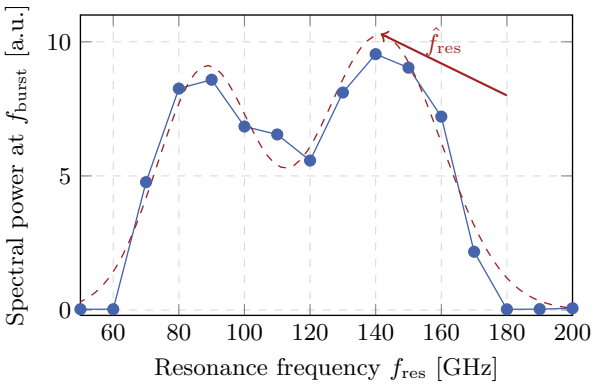

Figure 2: In the case without an additional impedance there is no emitted CSR below the unperturbed bursting threshold. Here however, an additional corrugation impedance with a resonance frequency of f_{res} leads to an emission of CSR, here plotted at the bursting frequency f_{burst}. A dashed line indicates the 2-peak Gaussian fit. Constant parameters are $Z_0 = 1\,\mathrm{k}\Omega$, $Q = 3$, $\alpha_c = 6 \times 10^{-4}$, and $V_{\mathrm{acc}} = 0.9\,\mathrm{MV}$.

at values that are suitable for a structure length of 20 cm [7] in this contribution: $Z_0 = 1\,\mathrm{k}\Omega$ and $Q = 3$.

For the design of the corrugated structure, the impact on the threshold current of the microbunching instability is a key parameter. In the unperturbed case, i.e. without the additional impedance, there is no CSR emission below the threshold current. To investigate to what extent the additional impedance can reduce the threshold current leading to emission of CSR, we simulated the emitted power for different resonance frequencies at a bunch current corresponding to 98.5 % of the unperturbed threshold current. The Fourier transform of this simulated emitted power over time reveals the dominant fluctuation frequencies of the microbunching. Figure 2 shows the emitted power at the dominant fluctuation frequency f_{burst} of the instability depending on the resonance frequency of the additional impedance for the machine settings $\alpha_c = 6 \times 10^{-4}$ and $V_{\mathrm{acc}} = 0.9\,\mathrm{MV}$. Since no significant amount of CSR power is emitted below the instability threshold current, the significant enhancement of the fluctuation power shown in the plot indicates a reduction of the threshold current for a certain range of the resonance frequency of the additional impedance. For the machine settings used in Figure 2, this reduction of the threshold current can be observed for an impedance resonance frequency in the range from 70 GHz to 170 GHz. For the determination of the impedance resonance frequency $\hat{f}_{\mathrm{res}}$ that is most effective at reducing the threshold current, the CSR power at f_{burst} versus f_{res} is fitted with a 2-peak Gaussian. Note that this double peak structure only appears for some machine settings, while the dependence resamples a simple Gaussian in the other cases.

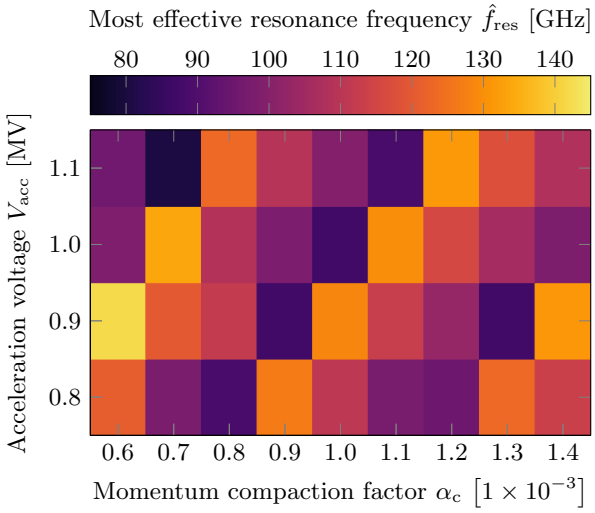

Figure 3: Color-coded most effective impedance resonance frequency $\hat{f}_{\mathrm{res}}$ of the maximal fluctuation power enhancement depending on the two machine parameters V_{acc} and α_c.

MACHINE SETTING SCANS

The impact of the corrugated structure on the longitudinal beam dynamics depends on the KARA machine settings. The investigation of this dependence is of great interest for the design of the corrugated plates and the understanding of the microbunching instability. Therefore, we performed a scan of the impedance resonance frequency for different values of V_{acc} and α_c at 98.5 % of the respective unperturbed threshold current.

This most effective resonance frequency $\hat{f}_{\mathrm{res}}$ is shown in Figure 3 as a function of both machine parameters. Increasing α_c shows that the single, dominant peak shifts to smaller f_{res} until it reaches the value of about 80 GHz, where it jumps back to $\hat{f}_{\mathrm{res}} \approx 135\,\mathrm{GHz}$. It decreases with increasing momentum compaction factor until a threshold value is reached and then jumps back to the maximal value. Additionally, it can be seen, that $\hat{f}_{\mathrm{res}}$ remains constant along the first diagonal. This behavior is based on the different shapes of the fluctuation power as the scan of f_{res} for the different machine settings shows. However, for understanding the phenomenon, the dependency on the beam properties is more relevant than that on machine settings. For this purpose, the machine settings are reduced to the dimensionless and accelerator-independent shielding parameter Π [10]:

$$\Pi = \frac{\rho^{\frac{1}{2}}}{2 \cdot h_{1/2}^{\frac{3}{2}}} \sigma_{z,0} \tag{2}$$

with bending radius ρ, half spacing between parallel plates $h_{1/2} = \frac{1}{2} h_c$. This parameter is proportional to the zero-current bunch length $\sigma_{z,0}$.

Figure 4 shows $\hat{f}_{\mathrm{res}}$ depending on this parameter, where different colors and shapes indicate the respective number of substructures in the longitudinal phase space that are

ISBN: 978-3-95450-231-8 ISSN: 2673-5490 doi: 10.18429/JACoW-IPAC2023-WEPL189

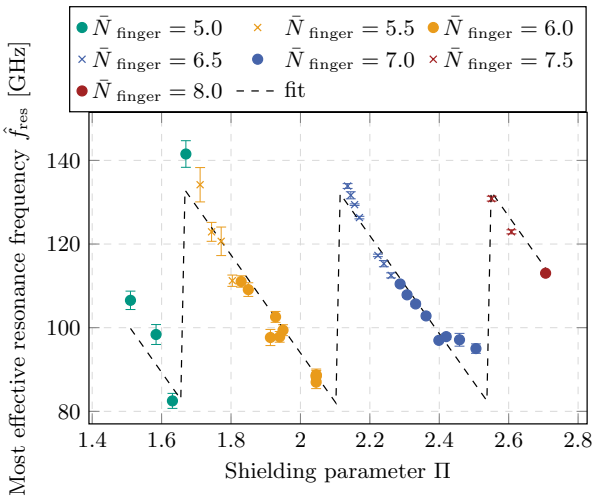

Figure 4: Most effective impedance resonance frequency $\hat{f}_{\text{res}}$ maximizing the fluctuation power depending on the shielding parameter $\Pi \propto \sigma_0$. The color indicates the number of substructures in the longitudinal phase space.

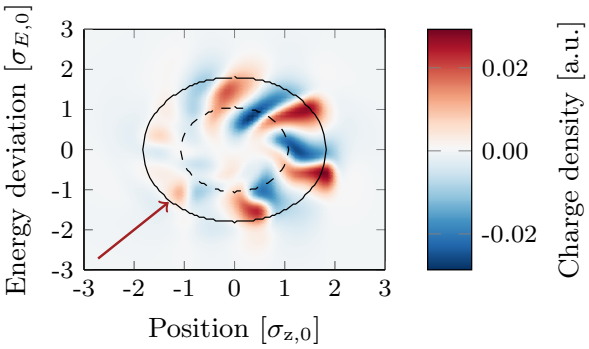

Figure 5: Example of the longitudinal phase-space with non-integer number of substructures ($\bar{N} = 5.5$) with the machine settings V_{acc}=0.9 MV and α_c=7 × 10^{-4}. By subtracting the mean temporal distribution, the substructures are more pronounced. Since the substructures start to develop from the outside (solid line) to the inside (dashed line) of the phase space, in the lower-left part, the additional finger (red arrow) is only present in the outer part.

caused by the microbunching instability. In this context, the half-integer finger numbers imply a different number of substructures in the inner and outer parts of the phase space. We show an example of a phase space with a half-integer number of fingers in Figure 5, which has been studied already by M. Brosi [12].

Figure 4 shows a clear saw-tooth behavior, which correlates directly with the number of fingers in the outer part of the phase space. Thereby, the second peak in the scan of the fluctuation power in dependence on the impedance resonance frequency (as seen in Fig. 2) is only significant in the transition range between the individual saw teeth. As long as the number of substructures is constant, $\hat{f}_{\text{res}}$ decreases linearly with the shielding parameter down to $\hat{f}_{\text{res,min}} = (82.9 \pm 3.2)$ GHz. As soon as the zero-current bunch length is long enough that an additional substructure can develop, the most effective resonance frequency jumps to the maximal value $\hat{f}_{\text{res,max}} = (132.8 \pm 1.4)$ GHz. T. Boltz has shown a similar periodic saw-tooth behavior [13] of the substructure oscillation frequency versus the shielding.

The fit with a saw-tooth function allows the determination of the necessary longitudinal space to form an additional substructure, which is given by periodicity $\Delta\Pi = (0.443 \pm 0.011)$ of the saw-tooth and accordingly $\Delta\sigma_0 = (1.260 \pm 0.031)$ ps for the KARA machine dimensions.

Beyond that, this periodic dependency of the most effective impedance structure on the bunch length gives the possibility of measuring the dimensions of the substructures indirectly by measuring the changes in the emitted intensity fluctuations as a function of the machine settings for a fixed additional impedance. This gives an understanding of the dominant frequency creating the longitudinal substructures, allowing a clearer insight into the microbunching instability.

SUMMARY & OUTLOOK

It is planned to install a versatile impedance manipulation chamber into the KARA storage ring to manipulate the longitudinal beam dynamics and, in this way, study the microbunching instability. The results of the beam dynamics simulation with the Vlasov-Fokker-Planck solver Inovesa show that the resonance frequency is the most crucial parameter of the impedance to manipulate the longitudinal beam dynamics.

The resonance frequency $\hat{f}_{\text{res}}$ most effective at reducing the threshold current of the microbunching instability varies in the range of 83 GHz to 133 GHz. Also, we observe a periodic dependency of $\hat{f}_{\text{res}}$ on the zero-current bunch length, determined by the number of substructures in the longitudinal phase space and bunch profile. Therefore, it is possible to use the identical impedance structure for different machine settings to influence the longitudinal beam dynamics effectively.

The production of prototypes is currently ongoing. Furthermore, the corrugated structures will be electrically characterized by measuring the S-parameters of electromagnetic waves with different frequencies.

ACKNOWLEDGEMENTS

This work is supported by the DFG project 431704792 in the ANR-DFG collaboration project ULTRASYNC.

S. Maier acknowledges the support by the Doctoral School "Karlsruhe School of Elementary and Astroparticle Physics: Science and Technology" (KSETA).

REFERENCES

[1] A.-S. Müller *et al.*, "Far Infrared Coherent Synchrotron Edge Radiation at ANKA", in *Proc. PAC'05*, Knoxville, TN, USA, May 2005, paper RPAE038, pp. 2518-2520.

ISBN: 978-3-95450-231-8 ISSN: 2673-5490 doi: 10.18429/JACoW-IPAC2023-WEPL189

[2] A. I. Papash *et al.*, "Non-Linear Optics and Low Alpha Operation at the Storage Ring KARA at KIT", in *Proc. IPAC'18*, Vancouver, Canada, Apr.-May 2018, pp. 4235–4238. doi:10.18429/JACoW-IPAC2018-THPMF070

[3] M. Venturini and R. Warnock, "Bursts of Coherent Synchrotron Radiation in Electron Storage Rings: A Dynamical Model", in *Phys. Rev. Lett. 89*, p. 224802, 2002. doi:10.1103/PhysRevLett.89.224802

[4] E. Roussel, C. Evain, C. Szwaj, S. Bielawski, j. Raasch, P. Thoma, A. Scheuring, M. Hofherr, K. Ilin, and S. Wünsch *et al.*,"Microbunching Instability in Relativistic Electron Bunches: Direct Observation of the Microstructures Using Ultrafast YBCO Detectors", in *Phys. Rev. Lett. 113*, p. 094801, 2014. doi:10.1103/PhysRevLett.113.094801

[5] K. Y. Ng *et al.*,"Explicit expressions of impedances and wake functions", Fermi National Accelerator Lab.(FNAL), Batavia, IL, USA, Rep. SLAC-PUB-15078, FERMILAB-FN-0901-APC, 2010. doi:10.2172/1002001

[6] V. S. Vladimirov, "Equations of mathematical physics", New York, Dekker, 1971, p.75.

[7] S. Maier, M. Brosi, A. Mochihashi, A.-S. Müller, M. J. Nasse, and M. Schwarz, "Impedance Studies of a Corrugated Pipe for KARA", in *Proc. IPAC'21*, Campinas, Brazil, May 2021, pp. 2039–2042. doi:10.18429/JACoW-IPAC2021-TUPAB251

[8] Inovesa, https://github.com/Inovesa

[9] P. Schönfeldt *et al.*,"Parallelized Vlasov-Fokker-Planck solver for desktop personal computers", in *Phys. Rev. Accel. Beams*, 2017. doi:10.1103/PhysRevAccelBeams.20.030704

[10] J. B. Murphy, R. L. Gluckstern, and S. Krinsky, "Longitudinal wakefield for an electron moving on a circular orbit", in *Part. Accel. 57*, 1997, https://cds.cern.ch/record/1120287/

[11] S. Maier *et al.*, "Simulation of the Effect of Corrugated Structures on the Longitudinal Beam Dynamics at KARA", in *Proc. IPAC'22*, Bangkok, Thailand, Jun. 2022, pp. 2241–2244. doi:10.18429/JACoW-IPAC2022-WEPOMS006

[12] M. Brosi, "In-Depth Analysis of the Micro-Bunching Characteristics in Single and Multi-Bunch Operation at KARA", Ph.D. thesis, KIT, 2020.

[13] T. Boltz, "Micro-Bunching Control at Electron Storage Rings with Reinforcement Learning", Ph.D. thesis, KIT, 2021.